Thickness distribution of Antarctic sea ice

Anthony P. Worby,[1] Cathleen A. Geiger,[2] Matthew J. Paget,[3] Michael L. Van Woert,[4] Stephen F. Ackley,[5] and Tracy L. DeLiberty[2]

[1] Ship-based observations are used to describe regional and seasonal changes in the thickness distribution and characteristics of sea ice and snow cover thickness around Antarctica. The data set comprises 23,373 observations collected over more than 2 decades of activity and has been compiled as part of the Scientific Committee on Antarctic Research (SCAR) Antarctic Sea Ice Processes and Climate (ASPeCt) program. The results show the seasonal progression of the ice thickness distribution for six regions around the continent together with statistics on the mean thickness, surface ridging, snow cover, and local variability for each region and season. A simple ridge model is used to calculate the total ice thickness from the observations of level ice and surface topography, to provide a best estimate of the total ice mass, including the ridged component. The long-term mean and standard deviation of total sea ice thickness (including ridges) is reported as 0.87 ± 0.91 m, which is 40% greater than the mean level ice thickness of 0.62 m. Analysis of the structure function along north/south and east/west transects revealed lag distances over which sea ice thickness decorrelates to be of the order of $100-300$ km, which we use as a basis for presenting near-continuous maps of sea ice and snow cover thickness plotted on a $2.5° \times 5.0°$ grid.

1. Introduction

[2] The Antarctic sea ice zone is not a uniformly level nor continuous sheet of ice. It comprises a complex mixture of different ice types and thicknesses, each with a variable thickness snow cover, and interspersed with an equally complex network of open water leads. The ice thickness distribution for a given region describes the relative abundance of each ice thickness category, and varies temporally as each category responds to thermal and mechanical forcing. In particular, the thin end of the thickness distribution is dominated by low strength and high growth rates, while the thicker, deformed ice in the distribution accounts for most of the sea ice mass [*Thorndike et al.*, 1975]. The aggregate properties of the pack ice and its interactions with the atmosphere and ocean are in many ways determined by the relative abundance of each ice type, and it is therefore important to know the distribution of ice thickness, and its regional and seasonal variability.

[1]Australian Antarctic Division and Antarctic Climate and Ecosystems Cooperative Research Center, Kingston, Tasmania, Australia.
[2]Department of Geography, University of Delaware, Newark, Delaware, USA.
[3]Commonwealth Scientific and Industrial Research Organization, Canberra, ACT, Australia.
[4]Office of Polar Programs, National Science Foundation, Arlington, Virginia, USA.
[5]Department of Earth Science and Environmental Sciences, University of Texas at San Antonio, San Antonio, Texas, USA.

[3] The initial growth of sea ice has the form of tiny ice crystals called frazil ice, which occur when the freezing point of seawater reaches approximately $-1.9°C$. Frazil crystals may form at the surface, or at depth, since an appreciable thickness of the water column is cooled to the freezing point by convective mixing [*Weeks and Ackley*, 1986]. These crystals subsequently coalesce at the surface to form grease ice or shuga depending on wind conditions and sea state, and eventually consolidate into either a level sheet of nilas (under calm conditions), or the distinctive patterns of pancake ice that occur when there is some wind or wave action [*World Meteorological Organization*, 1970]. Subsequent thickening occurs by thermodynamic growth, or by mechanically rafting and ridging ice floes, and it is this combination of processes that determines the ice thickness distribution. Mechanical processes redistribute the ice in a way that conserves total mass, thus accounting for the extremes in ice thickness by redistributing thin ice into thicker ridged categories, while simultaneously creating open water where new ice can form. Thermodynamic processes on the other hand are responsible for ice growth and melt, which result in a net gain or loss of mass respectively.

[4] In the Antarctic, annual fast ice tends to grow to a maximum thermodynamic thickness of $1.5-2.0$ m [*Heil et al.*, 1996], but in the more dynamic pack ice zone sea ice rarely grows thermodynamically to more than 0.3 m before it is deformed [e.g., *Allison and Worby*, 1994; *Jeffries et al.*, 1997; *Wadhams et al.*, 1987]. Ice growth rates are strongly affected by the magnitude of the heat fluxes at the top and

underside of the ice, as well as the thermal history of the ice, its thickness, snow cover and internal structure [*Thorndike et al.*, 1975]. The highest growth rates in Antarctica are typically observed in coastal polynyas where new ice may form under extreme winter conditions at up to 0.25 m d^{-1} [*Roberts et al.*, 2001], but are much lower in most regions of the Antarctic pack ice. Snow-related processes are also particularly important in the Antarctic [*Fichefet and Morales Marqueda*, 1999]; in particular the formation of snow ice that occurs when the base of the snow cover is flooded by sea water and refreezes to form ice. The prevalent flooding is attributable to several factors; one is the loading of the ice cover by the deposition of snow, depressing the top of the ice below sea level; another is that areas of thinner ice can be loaded down by the redistribution of the snow cover by wind [*Lange et al.*, 1990]. Additionally, the effects of ocean heat flux melting the under-side of the ice serves to not only thin the ice but also to lower the freeboard of thin sea ice with a snow cover below sea level and initiate flooding [*Lytle and Ackley*, 1996; *Maksym and Jeffries*, 2000].

[5] *Thorndike et al.* [1975] developed the governing equation for the ice thickness distribution of an area R, as

$$\frac{\partial g}{\partial t} = -\nabla \bullet (Vg) - \frac{\partial}{\partial h}(\xi g) + \psi, \qquad (1)$$

where g is the thickness distribution such that $g(h)$ is the fraction of a given area R covered by ice greater than thickness h but less than $h + dh$; V is the velocity field; ξ is the ice growth rate; and t is time. The first term on the right-hand side of equation (1) describes the advection and divergence of ice within area R. The second term is the thermodynamic growth term that describes the transfer of ice between thickness categories due to ice growth or melt. The third term, ψ, is the mechanical redistribution function that describes the creation of open water and the effects of rafting and ridging that transform thin ice into a range of thicker ice in a way that conserves ice volume within R. Generally, ξ is considered to be a function of $g(h)$, and ψ a function of both $g(h)$ and the rate of deformation. *Hibler* [1980] subsequently added a fourth term, $F_{lat}(g,h)$ to the right-hand side of equation (1) to include the effects of lateral melt which were neglected by *Thorndike et al.* [1975], such that

$$\int_0^\infty F_{lat}dh = 0, \qquad (2)$$

where F_{lat} is effectively a source and sink term such that $F_{lat} > 0$ for $h = 0$ and $F_{lat} < 0$ for $h > 0$. By definition, the lateral melt of ice will be compensated by an increase in the extent of open water.

[6] Numerous studies have shown that the distribution of thin ice and open water within the pack ice is important for determining other characteristics such as the compressive strength of the pack [e.g., *Hibler*, 1979], the turbulent and radiative heat exchange with the atmosphere [e.g., *Maykut*, 1978; *Worby and Allison*, 1991] and ice growth rates [e.g., *Hibler and Ackley*, 1983]. From the point of view of climate

modeling, an accurate representation of the ice thickness distribution is particularly important if these parameters are to be dealt with correctly. To date however there has been no Antarctic sea ice thickness climatology available to modelers, who instead have often used single mean averages (typically 0.5–1.0 m) over the majority of the Antarctic pack [e.g., *Flato*, 2004; *Hibler and Ackley*, 1983] with only limited validation from field measurements.

[7] In this paper we present ship-based observations to describe the regional and seasonal variability in Antarctic sea ice and snow cover thickness in six regions around Antarctica. It is hoped that this work will provide modelers and climatologists with some basis for the regional and seasonal validation of their models.

2. Data Description

[8] Since the days of the earliest explorers, ships' logs have recorded encounters with sea ice. Captain James Cook, the first to circumnavigate Antarctica in 1777, frequently reported the presence of sea ice as he tried to push south toward the continent, as did Captain Fabian von Bellingshausen during his exploration in 1831. The ice extent data from these log books were compared with the early passive microwave data by *Parkinson* [1990] but unfortunately the logs do not contain information on sea ice thickness. The same is true of the British Discovery Reports, from which *Mackintosh and Herdman* [1940] compiled a circumpolar map of the monthly variation of the average sea ice edge based on data from ships' logs during the 1920s and 1930s. These were later updated and republished by *Mackintosh* [1972]. In recent decades however, vessels have become more ice capable and spend more time south of the ice edge in support of logistic and scientific activities. Consequently the sea ice logs from these ships have become more comprehensive and often include an estimate of sea ice thickness, or ice type [*World Meteorological Organization*, 1970] from which thickness can be inferred.

[9] In the Arctic, declassified military data from upward-looking sonar aboard submarines have been used to study changes in sea ice thickness. Recent results have shown significant changes in the ice thickness distribution in different regions of the Arctic, with generally more thin ice and less thick, deformed ice in 1993–1997 than in 1958–1970 [*Rothrock et al.*, 1999, 2003; *Tucker et al.*, 2001; *Wadhams and Davis*, 2000; *Yu et al.*, 2004]. This coincides with a decrease in Arctic sea ice extent observed from satellite data over similar times, as reported in several studies [e.g., *Parkinson et al.*,1999; *Johannsen et al.*,1995; *Serreze et al.*, 2003, 2007]. In Antarctica the sea ice extent has shown considerable regional variability for the period 1979–1998, but with no statistically significant net change [*Comiso*, 2003]. Any changes in Antarctic sea ice thickness however would currently be going unnoticed, given the lack of a large-scale program of submarine observations in that region. Consequently it has been necessary to implement a ship-based program of routine observations for measuring Antarctic sea ice thickness, as reported here.

2.1. ASPeCt Data Set

[10] In 1997, the Scientific Committee on Antarctic Research (SCAR) established the Antarctic Sea Ice Pro-
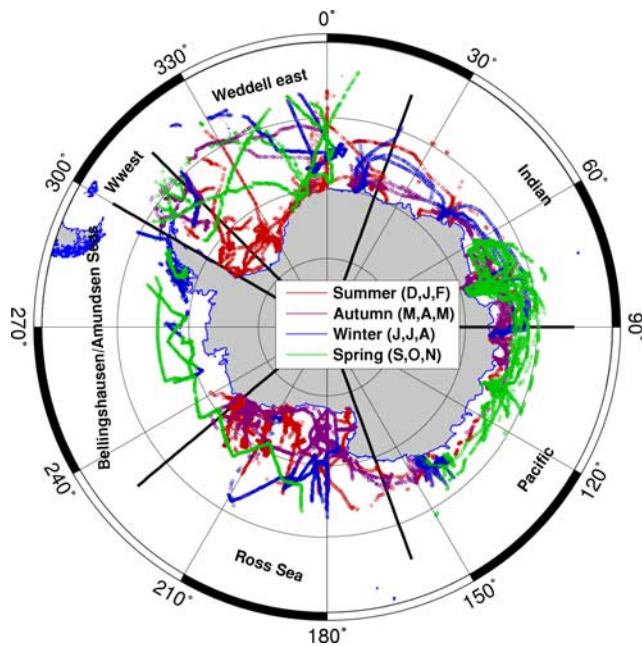
Figure 1. Map showing all data from 81 voyages and 2 helicopter flights. Seasonal separation is shown using different colors, where summer (DJF) is red, autumn (MAM) is purple, winter (JJA) is blue, and spring (SON) is green. The data plotted represent the 6 nautical mile subset of the full archive, representing 14,557 data points.

cesses and Climate (ASPeCt) program. One of the program's first objectives was to collate the many disparate sea ice logs kept from icebreakers operating in the Antarctic sea ice zone. This effort focused primarily on the Australian, German, US and Russian national Antarctic programs, which were known to have dozens of data sets containing information on the concentration, thickness and snow cover characteristics of the Antarctic sea ice zone. The data presented in this paper are a compilation of 21,710 individual ship-based observations collected from 81 voyages to Antarctica over the period 1981–2005, plus 1663 aircraft-based observations as described below. The ship-based observations are typically recorded hourly and include the ship's position, total ice concentration and an estimate of the areal coverage, thickness, floe size, topography, and snow cover characteristics of the three dominant ice thickness categories within a radius of approximately 1 km around the ship [*Worby and Allison*, 1999]. Not all observations contain this level of information, but at a minimum the partial ice concentrations and thicknesses (or ice types) were necessary for inclusion in the data set. The 81 voyages are summarized in Tables 1 and 2, with the location of each observation (colored by season) plotted in Figure 1. The data are publicly available via the ASPeCt website (http://www.aspect.aq) or from the Australian Antarctic Data Centre (http://www.data.aad.gov.au).

[11] Many of the individual data sets have already been described in published papers and reports [e.g., *Allison and Worby*, 1994; *Casarini*, 1992], but required a significant amount of work to translate them into a consistent, quality-controlled format. Many other data sets were still in the
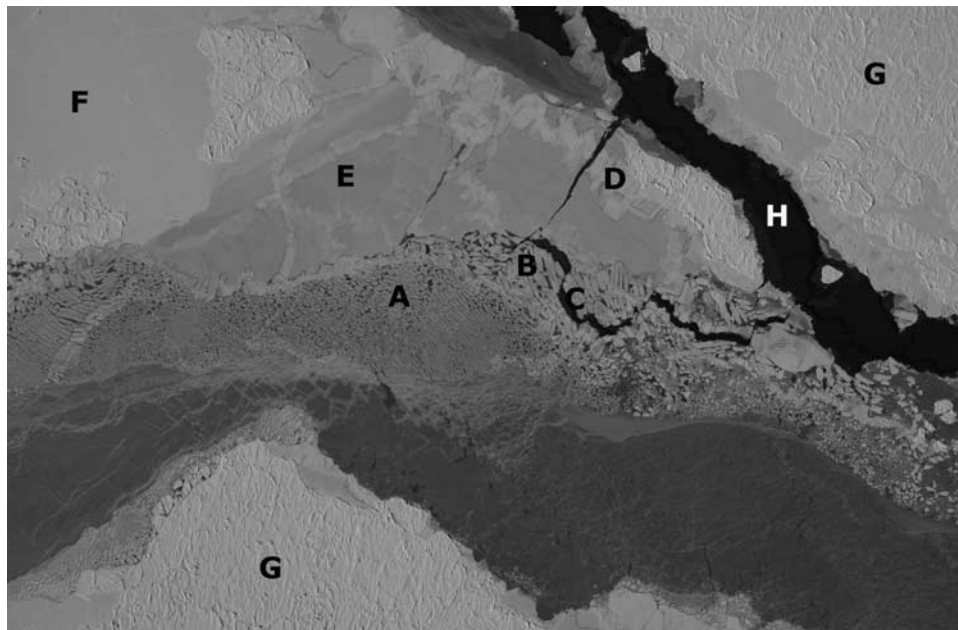

Figure 2. Aerial photograph over east Antarctic sea ice showing the range of ice types that can occur within a small area. The thin ice at A has been broken into tiny floes by wave action, some of which have subsequently refrozen together (B) before being split apart again by the formation of a new lead (C). The effects of finger rafting can be seen in the grey-white nilas (D), while steady thermodynamic growth has formed new grey-white (E) and first-year (F) ice. Older, thicker floes (G) have clearly undergone significant deformation and have a variable thickness snow cover, while new grease ice is forming in the leads (H). The image is approximately 1200 × 800 m in size with a resolution of approximately 0.4 m.

Table 1. Details of Each Voyage on Which Sea Ice Observations Were Made, and That Have Been Contributed to the ASPeCt Data Archive[a]

Vessel	Dates in Ice	Region	Voyage ID	Observations
Mikhail Somov	Feb 1981	140°W–136°W	26th Russian expedition	59
Mikhail Somov	Feb–March 1982	142°W–134°W	27th Russian expedition	111
Mikhail Somov	Feb–March 1984	145°W–127°W	29th Russian expedition	160
Mikhail Somov	March–Aug 1985	153°W–134°W	30th Russian expedition	328
Mikhail Somov	Feb–March 1986	151°W–137°W	31st Russian expedition	150
Mikhail Somov	Feb 1987	145°W–133°W	32nd Russian expedition	142
Akademic Fedorov	Feb–March 1988	164°W–121°W	33rd Russian expedition	88
Polarstern	Oct–Nov 1988	55°W–45°W	ANT VII/1 (EPOS)	115
Akademic Fedorov	Feb–March 1989	176°W–138°W	34th Russian expedition	152
Polarstern	Sept–Oct 1989	59°W–8°E	ANT VIII/2 (WWGS)	398
Mikhail Somov	Feb–March 1090	176°E–134°W	35th Russian expedition	240
Akademic Fedorov	March 1990	175°W–131°W	35th Russian expedition	371
Akademic Fedorov	Dec 1990 to Jan 1991	23°E–95°E	36th Russian expedition	188
Akademic Fedorov	Nov 1991 to Jan 1992	34°E–94°E	37th Russian expedition	929
Akademic Fedorov	Jan–Feb 1992	50°W–1°W	37th Russian expedition	347
Akademic Fedorov	March–April 1992	13°E–102°E	37th Russian expedition	342
Nathaniel B. Palmer	May 1992	56°W–48°W	NBP 92-1 (ISW)	104
Akademic Fedorov	May–June 1992	60°W–16°W	37th Russian exp (ISW)	714
Aurora Australis	Oct–Nov 1992	60°E–85°E	Voyage 1 92/93	203
Akademic Fedorov	Jan–Feb 1993	72°E–119°W	38th Russian expedition	184
Aurora Australis	March 1993	139°E–141°E	Voyage 9.0 92/93	13
Akademic Fedorov	March–April 1993	60°W–95°E	38th Russian expedition	226
Aurora Australis	April–May 1993	140°E–150°E	Voyage 9.1 92/93	54
Nathaniel B. Palmer	Aug–Sept 1993	110°W–83°W	NBP 93-5	225
Aurora Australis	Oct–Nov 1993	62°E–115°E	Voyage 2 93/94	144
Akademic Fedorov	Dec 1993 to Feb 1994	2°W–160°W	39th Russian expedition	210
Mikhail Somov	Jan–Feb 1994	9°E–93°E	39th Russian expedition	126
Akademic Fedorov	March–April 1994	73°E–100°E	39th Russian expedition	269
Mikhail Somov	March–May 1994	58°W–78°E	39th Russian expedition	430
Nathaniel B. Palmer	July–Aug 1994	31°W–5°E	NBP 94-4 (ANZFLUX)	361
Aurora Australis	Sep–Oct 1994	74°–150°E	Voyage 1 94/95	338
Nathaniel B. Palmer	Sept–Oct 1994	172°–107°W	NBP 94-5	520
Aurora Australis	Oct–Nov 1994	73°–112°E	Voyage 1 94/95	246
Akademic Fedorov	Jan–March 1995	11°–93°E	40th Russian expedition	140
Mikhail Somov	March–April 1995	10°–77°E	40th Russian expedition	240
Nathaniel B. Palmer	March–April 1995	143°–169°E	NBP 95-2	113
Aurora Australis	April 1995	110°–127°E	Voyage 7 94/95	24
Akademic Fedorov	April–May 1995	10°–93°E	40th Russian expedition	506
Nathaniel B. Palmer	May–June 1995	180°W–165°W	NBP 95-3	481
Aurora Australis	July–Aug 1995	138°E–143°E	Voyage 1 95/96 (HIHO)	186
Nathaniel B. Palmer	Aug 1995	180°W–149°W	NBP 95-5a	315
Nathaniel B. Palmer	Aug–Sept 1995	110°W–77°W	NBP 95-5b	291
Kapitan Khlebnikov	Nov 1995	44°W–8°W	tourist vessel	160
Polarstern	Dec 1995	9°W–0°W	ANT XIII/2 (SO-JGOFS)	45
Akademic Fedorov	May–July 1996	31°W–93°E	41st Russian expedition	775
Polarstern	Jan–Feb 1997	57°W–8°W	ANT XIV/3	136
Akademic Fedorov	May–July 1997	10° E–93°E	42nd Russian expedition	819
Aurora Australis	Oct 1997	65°–110°E	Voyage 2 97/98	137
Endurance Endurance voyage (Jan – Feb 1998) has 635 ship observations and 206 helicopter observations.	Jan–Feb 1998	60°–9°W	Ronne Polyna (ROPEX)	841
Akademic Fedorov	Feb–March 1998	38°–96°E	43rd Russian expedition	217
Akademic Fedorov	April–June 1998	10°–96°E	43rd Russian expedition	387
Nathaniel B. Palmer	May–June 1998	164°E–175°W	NBP 98-3	405
Aurora Australis	July 1998	143°–148°E	Voyage 1 98/99	31
Aurora Australis	Nov–Dec 1998	71°–113°E	Voyage 4 98/99	488
Nathaniel B. Palmer	Dec 1998 to Jan 1999	166°–134°W	NBP 99-1	241
Polar Sea	Dec 1998 to Jan 1999	140°E–174°W	US Coast Guard	76
Polarstern	Jan–March 1999	62°W–0°W	ANT XVI/2	699
Aurora Australis	March 1999	63°E–77°E	Voyage 6 98/99	60
Nathaniel B. Palmer	June–July 1999	80°W–68°W	NBP 99-6 (LTER)	110
Aurora Australis	July–Aug 1999	141°E–148°E	Voyage 1 99/00 (MGP)	700
Nathaniel B. Palmer Nathaniel B. Palmer voyage (Dec 1999 – Feb 2000) has 497 ship observations and 1457 helicopter observations.	Dec 1999 to Feb 2000	180°W–129°W	NBP 99-9 (APIS)	1954
Kapitan Khlebnikov	Nov 1999	109E 144°E	Voyage 2.1 99/00	75
Aurora Australis	Dec 1999 to Jan 2000	62°E–154°E	Voyage 4 99/00 (APIS)	415
Aurora Australis	Feb 2000	109°E–112°E	Voyage 5 99/00	19

Table 1. (continued)

Vessel	Dates in Ice	Region	Voyage ID	Observations
Polar Bird	Nov–Dec 2000	108°E–111°E	Voyage 3 00/01	54
Polarstern	Dec 2000	9°W–2°E	ANT XVIII/3	95
Shirase	Dec 2000 to Feb 2001	38°E–85°E	JARE 42 Syowa resupply	219
Lawrence M. Gould	July–Aug 2001	72°W–63°W	LMG 01-6 (SO-GLOBEC)	224
Nathaniel B. Palmer	July–Aug 2001	76°W–67°W	NBP 01-4 (SO-GLOBEC)	220
Nathaniel B. Palmer	Sept–Oct 2001	72°W–62°W	NBP 01-5 (LTER)	295
Aurora Australis	Nov–Dec 2001	139°E–145°E	Voyage 3 01/02	59
Lawrence M. Gould	Aug–Sep 2002	77°W–61°W	LMG 02-5 (SO-GLOBEC)	236
Nathaniel B. Palmer	Dec 2002	164°E–174°W	NBP 02-9	251
Polarstern	Dec 2002 to Jan 2003	8°W–26°E	ANT XX/2	287
Nathaniel B. Palmer	March–April 2003	158°E–180°E	NBP 03-2 (ANSLOPE)	429
Aurora Australis	Sept–Oct 2003	108°E–126°E	Voyage 1 03/04 (ARISE)	211
Nathaniel B. Palmer	Feb–April 2004	166°E–189°E	NBP 04-2 (ANSLOPE)	519
Aurora Australis	Oct–Nov 2004	107°E–126°E	Voyage 1 04/05	48
Polarstern	Nov 2004 to Jan 2005	56°W–14°W	ANT XXII/2 (ISPOL)	232
Polarstern	Feb–March 2005	55°W–1°E	ANT XXII/3	114
Nathaniel B. Palmer	July–Sep 2005	7°W–6°E	NBP 05-06 (MaudNESS)	307

[a]See Table 2 for a description of acronyms.

form of old analogue charts that have never been published, while others, even if digitized, were stored across multiple software applications using different formats, codes and abbreviations. A total of 17 voyages were excluded from the archive because of known inconsistencies or biases in the data or because of deficiencies such as a lack of topography data. This new ASPeCt data archive is circumpolar in nature and complements many of the regionally focused experiments that have yielded valuable ice thickness information using techniques such as upward-looking sonar [*Strass and Fahrbach*, 1998; *Worby et al.*, 2001], ship- and aircraft-based electromagnetic measurements [*Haas*, 1998; *Reid et al.*, 2003], and in situ drill-hole measurements [*Wadhams et al.*, 1987; *Lange and Eicken*, 1991; *Jeffries and Weeks*, 1992; *Worby et al.*, 1996, 1998].

[12] Figure 2 is an aerial photograph over Antarctic sea ice showing the range of ice conditions that can occur over an area of 1km, which is the approximate coverage of an ASPeCt ice observation. The scene represents the net effect of dynamic and thermodynamic processes that have influenced the evolution of the ice. The ASPeCt observing scheme cannot capture all the complexity of this scene, but does provide the capability to record the characteristics of the three dominant ice classes and their topography, floe size and snow cover characteristics. The thickness of each ice class cannot be determined from an aerial photograph, but can be quite accurately estimated from a ship as it cuts through the ice. A simple but highly effective method to help gauge the thickness of the ice is to suspend a fishing buoy of known diameter (usually – 0.5 m) over the side of the ship approximately 1–2 m above the ice surface. The thickness is estimated on the level parts of floes when they are broken and turned sideways along the hull of the ship. The topography is recorded separately as the percentage of area covered by ridges and the mean sail height. On some ships a purpose-built rule, with 20-cm graduations marked on it, is extended from the side of the ship to gauge the thickness of the turned blocks. The data are recorded on a log sheet and then digitized using purpose-built software that performs a suite of on-the-spot error checks [*Worby and Dirita*, 1999]. A training CD-ROM "Observing Antarctic

Sea Ice" [*Worby*, 1999] has been produced to ensure that observers are well trained and that observations are made consistently on different ships. A full description of the observational technique, data quality control, and data processing is presented in a technical report by *Worby and Allison* [1999].

[13] To avoid biasing, i.e., to ensure that each observation is independent, the ASPeCt data set has been edited to exclude observations within 6 nautical miles (nm) of the previous observation. This reduces the number of observations used in this paper from 23,373 to 14,557. This separation criterion is based on a ship speed of 6 knots which most icebreakers would maintain in undeformed first-year ice and is consistent with past analyses of ship-based data published by *Allison et al.* [1993], *Worby et al.* [1998] and *Brandt et al.* [2005]. Some helicopter data are also included in the archive. These were collected during two voyages; one to the Weddell Sea aboard *Endurance* from January through February 1998; and one to the Ross Sea aboard *Nathaniel B. Palmer* from December 1999 through February 2000. On the *Endurance* voyage, visual observations were made from the helicopter at 6 nautical mile spacing in the same manner as would normally occur from a vessel. On the *Nathaniel B. Palmer*, digital video was recorded continuously from the helicopter. The video tapes were analyzed for floe size, ice type, ice concentration and the fractional coverage of ridges at regular intervals along the flight lines (consistent with the minimum spacing of ship observations of 6 nautical miles), then combined with ice thickness, snow thickness and ridge sail height information based on observations from the ship [*Knuth and Ackley*, 2006]. The aircraft observations have helped to provide coverage in some of the thicker ice areas which ships may have difficulty accessing.

2.2. Sea Ice Deformation

[14] The ship-based observations record information on the level ice thickness (Z_u), the fractional coverage of ridges (R) and the average sail height of ridges (S) for up to three distinct ice thickness categories or ice "types." Together, these represent six distinct ice thicknesses, plus open water, that provide a good description of the ice thickness distri-
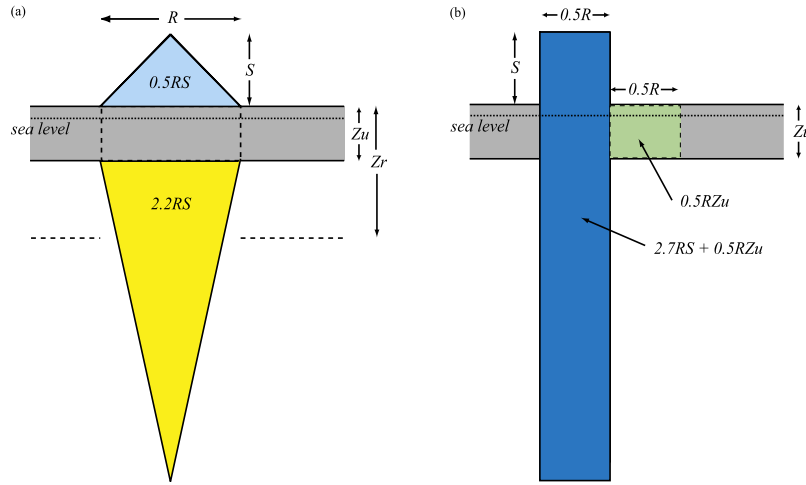
Figure 3. (a) Schematic of the model ridge structure, and the components of an ice floe observed as part of the ASPeCt protocol. (b) Schematic of the numerically modified ridge structure used for the ice thickness distribution analysis.

bution in the vicinity of the ship at the time the observation is made. We have developed a model to calculate the mean thickness (Z_r) of each ice thickness category based on the observations, such that

$$Z_r = 2.7RS + Z_u. \tag{3}$$

[15] Figure 3a shows the three components of the theoretical ridge structure, based on the observations, which include (1) a triangular sail with a cross-sectional area $0.5RS$ (light blue); (2) level ice in isostatic balance (grey); and (3) a keel component with a cross-sectional area $2.2RS$ (yellow). This configuration yields a keel depth to sail height ratio of 4.4 as determined from drilled measurements described in more detail in Appendix A. The first term on the RHS of equation (3) is the combined sail and keel components of the ice, while the second term represents the level ice component. The assumption of a triangular cross section is consistent with the formulation of *Hibler et al.* [1974] for calculating the effective thickness of ridged ice. Their formulation used a fixed slope angle of 26°, however we use an implied variable slope angle which is dependent on the fractional coverage of ridges and the average sail height. In this way, broader ridges are flatter, which is consistent with the theory that ridges should build laterally once the limiting height is reached [*Tucker and Govoni*, 1981], although it is well known that the shape of individual keels may vary enormously in both the Arctic and Antarctic [*Haas*, 2003].

[16] The level ice component of each ice type can also be separated into two sections as follows:

$$Z_u = RZ_u + (1 - R)Z_u, \tag{4}$$

where RZ_u is the slab of level ice between the ridge sail and keel that is essentially part of the ridge structure. It therefore follows that

$$Z_r = R(2.7S + Z_u) + (1 - R)Z_u, \tag{5}$$

where the first term on the RHS is the mean ridge thickness and the second term is the mean thickness of the level ice.

[17] To correctly represent the different ice thickness categories in the thickness distribution, we do not use the mean value Z_r (a value which is not physically representative), but instead redefine the shape of ridges as shown in Figure 3b. This effectively redefines the statistical distribution of ridges, reducing the percent coverage of ridges by half, but ensuring the thickness categories reported in the observations are those included in the statistical analysis. To conserve mass we re-assign half of the level ice between the ridge sail and keel (shown in green) back to the level ice component, and rewrite equation (5) as

$$Z_r = \frac{R}{2}(5.4S + Z_u) + \left(1 - \frac{R}{2}\right)Z_u, \tag{6}$$

where the first term on the RHS is a realistic thickness of the ridge and the second term is a realistic thickness of the level ice. It is these values that are used to compile

Table 2. Acronyms

Acronym	Full Name
ANSLOPE	Cross-slope Exchanges at the Antarctic Slope Front
ANZFLUX	Antarctic Zone Flux Experiment
APIS	Antarctic Pack Ice Seals Survey
ARISE	Antarctic Remote Ice Sensing Experiment
ASPeCt	Antarctic Sea Ice Processes and Climate
EPOS	European Polarstern Study
HIHO	Harmonious Ice and Hydrographic Observations
ISPOL	Ice Station Polarstern
ISW	Ice Station Weddell
LTER	Long Term Ecological Research
MaudNESS	Maud Rise Non-linear Equation of State Study
MGP	Mertz Glacier Polynya Experiment
ROPEX	Ronne Polynya Experiment
SO-GLOBEC	Southern Ocean–Global Ocean Ecosystems Dynamics
SO-JGOFS	Southern Ocean–Joint Global Ocean Flux Study
WWGS	Winter Weddell Gyre Study

Table 3. Summary Statistics of Sea Ice Variables for Each Region and Season Around Antarctica[a]

Sector	Number of Observations	Ice Concentration (Tenth), Mean (std)	Level Ice Thickness, m, Mean (std)	Average Ice Thickness, m, Mean (std)	Percent Ridging, Mean (std)	Ridge Height, m, Mean (std)	Snow Thickness, m, Mean (std)	Local Variability Eo, m²
			Annual					
Circumpolar	14557	6.9 (3.5)	0.62 (0.67)	0.87 (0.91)	12 (15)	0.57 (0.33)	0.16 (0.20)	0.64
Ross Sea	4155	6.7 (3.6)	0.84 (0.87)	1.07 (1.04)	11 (14)	0.57 (0.29)	0.24 (0.26)	0.84
Bell/Amund	1160	8.1 (2.8)	0.63 (0.67)	0.90 (0.87)	12 (15)	0.57 (0.33)	0.18 (0.19)	0.54
Weddell (west)	810	6.5 (3.7)	0.91 (0.75)	1.33 (1.13)	16 (19)	0.73 (0.43)	0.19 (0.24)	1.09
Weddell (east)	3128	6.5 (3.7)	0.50 (0.44)	0.73 (0.78)	11 (15)	0.61 (0.39)	0.11 (0.13)	0.53
Indian	3069	7.2 (3.4)	0.43 (0.36)	0.68 (0.70)	12 (16)	0.52 (0.28)	0.11 (0.12)	0.55
West Pacific	2235	7.2 (3.3)	0.54 (0.62)	0.79 (0.87)	12 (16)	0.54 (0.32)	0.15 (0.20)	0.49
			Summer					
Circumpolar	5006	4.6 (3.6)	0.91 ± 0.90)	1.17 (1.12)	11 (16)	0.63 (0.33)	0.24 (0.26)	0.87
Ross Sea	2194	5.0 (3.6)	1.12 (1.04)	1.32 (1.18)	8 (12)	0.60 (0.32)	0.34 (0.28)	0.84
Bell/Amund	138	5.3 (3.3)	1.91 (1.03)	2.14 (1.04)	11 (10)	0.59 (0.21)	0.50 (0.25)	0.63
Weddell (west)	409	5.3 (3.9)	0.82 (0.88)	1.20 (1.28)	14 (19)	0.69 (0.39)	0.16 (0.30)	1.42
Weddell (east)	1277	3.8 (3.6)	0.58 (0.55)	0.87 (0.99)	12 (18)	0.66 (0.38)	0.12 (0.16)	0.98
Indian	618	4.4 (3.4)	0.72 (0.48)	1.05 (0.84)	14 (18)	0.64 (0.29)	0.16 (0.16)	0.62
West Pacific	370	4.4 (3.3)	0.89 (0.87)	1.17 (1.05)	12 (16)	0.64 (0.27)	0.28 (0.23)	0.63
			Autumn					
Circumpolar	3758	7.9 (3.1)	0.44 (0.51)	0.68 (0.78)	12 (16)	0.51 (0.26)	0.10 (0.15)	0.26
Ross Sea	1374	8.3 (2.7)	0.52 (0.51)	0.82 (0.83)	14 (17)	0.54 (0.26)	0.13 (0.17)	0.41
Bell/Amund	42	–	–	–	–	–	–	–
Weddell (west)	199	7.6 (3.4)	0.98 (0.60)	1.38 (0.91)	18 (20)	0.58 (0.29)	0.19 (0.13)	0.48
Weddell (east)	560	7.8 (3.1)	0.29 (0.30)	0.44 (0.50)	9 (13)	0.43 (0.21)	0.05 (0.07)	0.15
Indian	1092	7.6 (3.3)	0.27 (0.22)	0.45 (0.43)	11 (15)	0.47 (0.19)	0.07 (0.07)	0.16
West Pacific	491	8.0 (3.1)	0.49 (0.80)	0.75 (1.10)	12 (17)	0.51 (0.36)	0.11 (0.24)	0.38
			Winter					
Circumpolar	2754	8.9 (2.0)	0.43 (0.32)	0.66 (0.60)	12 (15)	0.54 (0.26)	0.11 (0.12)	0.16
Ross Sea	420	9.4 (1.6)	0.49 (0.29)	0.72 (0.53)	11 (12)	0.54 (0.25)	0.15 (0.14)	0.07
Bell/Amund	495	8.5 (2.5)	0.39 (0.22)	0.65 (0.58)	12 (16)	0.53 (0.33)	0.11 (0.10)	0.28
Weddell (west)	39	–	–	–	–	–	–	–
Weddell (east)	610	8.9 (2.0)	0.40 (0.23)	0.54 (0.37)	9 (11)	0.49 (0.20)	0.08 (0.06)	0.05
Indian	583	9.0 (2.0)	0.38 (0.22)	0.59 (0.41)	13 (13)	0.50 (0.16)	0.12 (0.10)	0.12
West Pacific	607	9.0 (1.9)	0.44 (0.42)	0.72 (0.75)	13 (19)	0.59 (0.32)	0.12 (0.17)	0.16
			Spring					
Circumpolar	3039	7.7 (2.9)	0.53 (0.38)	0.81 (0.74)	11 (14)	0.60 (0.43)	0.15 (0.14)	0.42
Ross Sea	167	8.9 (1.6)	0.52 (0.16)	0.67 (0.30)	8 (8)	0.57 (0.29)	0.18 (0.08)	0.06
Bell/Amund	485	8.9 (2.1)	0.50 (0.36)	0.79 (0.76)	13 (15)	0.58 (0.37)	0.17 (0.13)	0.36
Weddell (west)	163	7.2 (2.9)	0.93 (0.53)	1.33 (0.85)	12 (11)	0.95 (0.59)	0.24 (0.19)	0.38
Weddell (east)	681	8.2 (2.4)	0.63 (0.35)	0.89 (0.64)	11 (15)	0.74 (0.52)	0.16 (0.12)	0.26
Indian	776	7.4 (3.0)	0.46 (0.34)	0.78 (0.87)	13 (15)	0.49 (0.39)	0.13 (0.14)	0.69
West Pacific	767	6.6 (3.3)	0.48 (0.39)	0.68 (0.62)	10 (14)	0.47 (0.29)	0.13 (0.14)	0.32

[a]The columns, from left to right, represent the sector, total number of observations, mean ice concentration, mean level ice thickness, mean total thickness including ridges, percentage of surface ridging, average ridge height above the surface of the level ice, mean snow thickness over the level ice and the local variability. Standard deviations for most parameters are shown in brackets.

the ice thickness distributions presented in this paper. We note that the level ice for a thicker type and a ridged value for a thinner type may have the same thickness and, if so, will be correctly binned together in compiling the thickness distribution under this scheme.

2.3. Snow Thickness

[18] The ASPeCt observations record only the snow thickness over level sea ice and therefore do not reflect the extremes that may occur in areas of ridging. The observing protocol involves recording the thickness and snow cover characteristics over the level portion of ice floes, but unlike sea ice thickness we do not have the observations or model input to correct these values for areas of ridging. Consequently, the snow thickness data presented

in this paper must be taken as a lower bound, and only representative for the level sea ice within the pack. This is discussed further by *Worby et al.* [2008].

2.4. Errors

[19] For ice thickness, the accuracy of careful ship-based observations will vary with the thickness of the ice floe being observed. On the basis of comparisons with drilled measurements the error associated with thin ice such as nilas and grey-white ice <10 cm thick, is ±50%; for ice between 0.1 and 0.3 m the error is ±30%; and for level ice >30cm the error is ±20%. These errors are estimates that are independent at each point and therefore spatially decorrelated. Similar error estimates apply for snow of the same thickness. For ice concentration, which is estimated in
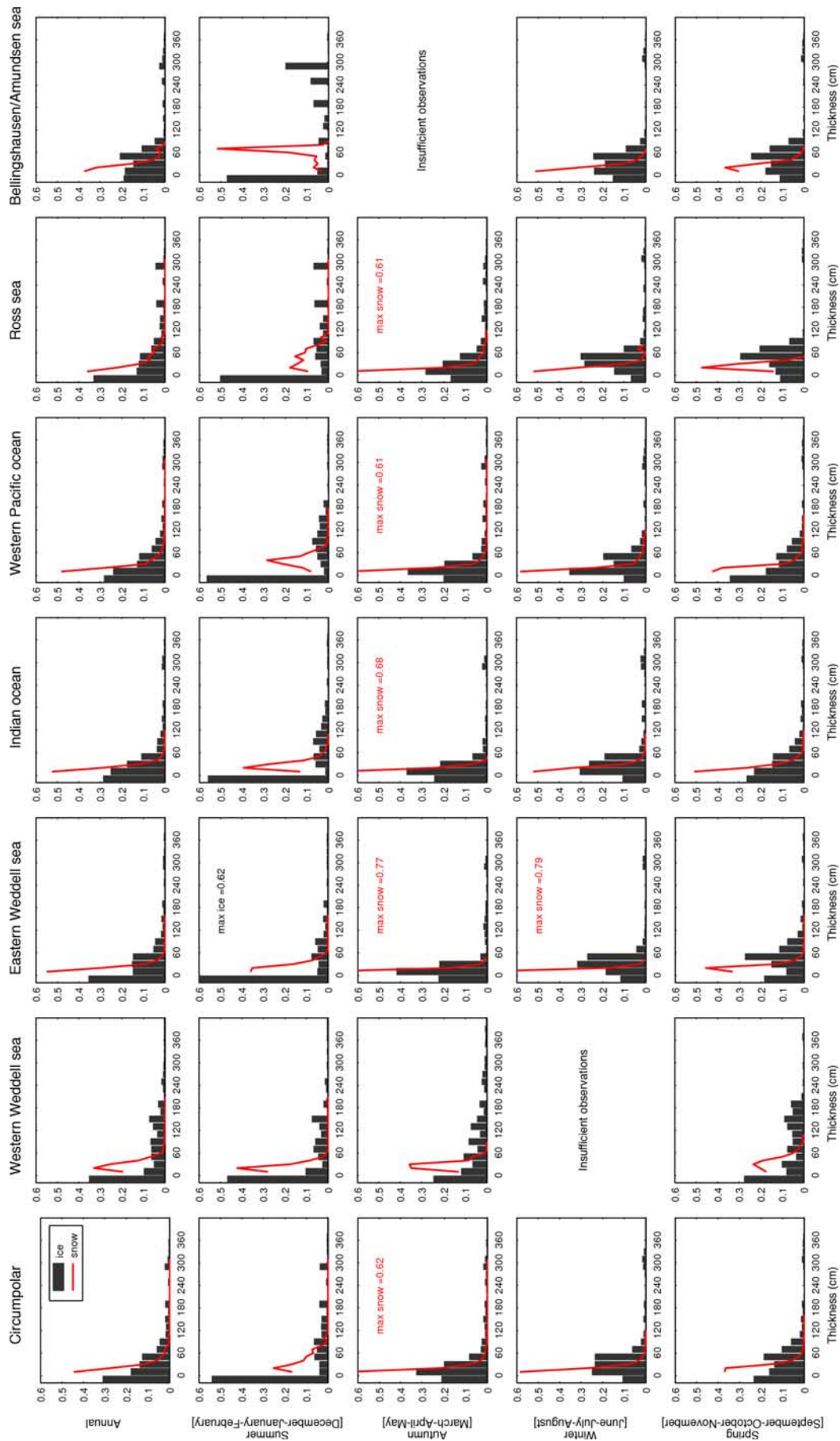
Figure 4. Ice and snow thickness distributions for each region and season. The ice thickness distributions are binned into 0.2-m-thickness intervals and are shown by black bars, including the open water fraction in the first column. The snow thickness distributions are binned into 0.1-m-thickness intervals and are shown as a red line. Where a thickness category value goes beyond the plotted limit of the y axis the exact number is shown in small print in the plot.

tenths, the accuracy is ±1 tenth, and this applies to the total concentration as well as to the partial concentrations of each ice type. *Knuth and Ackley* [2006] showed that point estimates by eye (similar to a ship-based visual observation) from digital video along a flight track gave very similar ice concentration values to an objective digital analysis of the entire track length using image processing software, based on the analysis of nine flights in the Ross Sea pack ice zone. This provides verification that visual point sampling along a track provides a good representation of ice concentration when compared with continuous measurements. *Geiger* [2006] presents a systematic technique for quantifying the uncertainty in ship-based data, describing the basic rules of error propagation in the context of the ASPeCt observing protocols.

[20] The average sail height (*S*) of ridges, and percentage of the area (*A*) covered by them, can be difficult to estimate and we assign an error to each of these of ±50%. It is very important that observers make these estimates by looking in the immediate vicinity of the ship, because looking toward the horizon can easily result in an overestimate of the amount of ridging when the level ice between ridges cannot easily be seen. Similarly, the vertical perspective from the ship's bridge can cause problems when estimating ridge height, so observers must "calibrate" their eye from in situ measurements on the ice or make observations of ridge height from a lower deck on the ship, to ensure that the observations are as accurate as possible.

[21] One source of error that is often raised in the context of ship-based observations is the bias caused by vessels choosing easily navigable routes that avoids regions of thick ice. This is a potential problem in areas of multiyear ice, such as the western Weddell Sea and eastern Ross Sea, which may be thicker than the capability of most ice-breakers. Often however, ships can penetrate these regions by following open water leads and record detailed information on the thicker ice in the region. A ship following a lead between thick floes will record the details of the surrounding ice, not just the open water. Consequently, accessibility is not so much restricted by ice thickness in these regions, as by ice concentration. The helicopter observations from the western Weddell and eastern Ross Seas also help to overcome issues of data coverage in these regions. Most of the rest of the Antarctic pack ice is within the capability of modern ice breakers, thereby minimizing the effects of ship track bias. While we acknowledge that the path of least resistance is usually preferable, it is often not necessary for ships to preferentially follow leads through much of the Antarctic pack, thereby providing ample opportunity for conducting observations. Conversely, the data may be biased in regions of thicker ice, which is why we employ the minimum-distance criteria of 6 nautical miles between consecutive hourly observations, as described above.

3. Data Analysis and Results

[22] Figure 1 shows the six sectors commonly used to describe regional variability in the Antarctic sea ice zone. These are the Ross Sea (160°E–130°W), Bellinghausen-Amundsen Sea (130°W–60°W), western Weddell Sea (60°W–45°W), eastern Weddell Sea (45°W–20°E), Indian Ocean (20°E–90°E), and Western Pacific (90°E–160°E)

sectors. The western Weddell Sea sector is identified separately because it contains as much as 80% of the multiyear ice around the Antarctic continent and is largely ice-covered year round [*Gloersen et al.*, 1992], while the eastern Weddell Sea sector is much more seasonal and essentially ice-free during summer. Table 3 provides the total number of observations in each of these sectors for each season after the 6 nautical mile editing has been applied. The seasons are defined as summer (DJF), autumn (MAM), winter (JJA) and spring (SON) as well as an annual average (ALL). We also present hemispheric values representative of the entire circumpolar sea ice zone.

3.1. Sea Ice and Snow Thickness Distributions

[23] The sea ice in different sectors of the Antarctic pack may exhibit significantly different characteristics and this is reflected in the ice and snow thickness distributions presented in Figure 4. The black histogram bars in Figure 4 show the ice thickness distribution (in 0.2 m bins), including the open water fraction, while the red lines show the snow thickness distribution (in 0.1 m bins) for the ice covered area. Data sparse regions (less than 100 observations in any given season) are not shown. Together with the statistics presented in Table 3, the thickness distributions shown in Figure 4 reveal some important characteristics of the pack ice zone.

3.1.1. Seasonal Variability

[24] Overall, summer is the period of extremes. It is the period when the mean ice thickness values are greatest while the mean ice concentration is lowest, reflecting the fact that only a small percentage of thin ice is present at this time of year. The standard deviations are also greatest in most regions in summer indicating the period of greatest variability in ice thickness. In autumn there is a pronounced increase in the amount of thin ice in all regions, with ice <0.4 m accounting for 50–60% of the pack. The redistribution of this thinner ice into thicker categories from autumn through summer is clearly visible in the distribution curves in Figure 4.

[25] The highest ice concentrations, with lowest variability, are seen in winter when leads are rapidly refrozen and the pack ice is kept close to 90% ice cover. There is some evidence of a bimodal distribution in some regions in winter and spring, which is most likely the result of deformation. Spring and autumn are the transition seasons and therefore quite similar in concentration, although the character of the pack ice is quite different. There is clearly more new ice in autumn and more deformed ice in spring which is reflected in both the mean ice thickness values for these seasons and the fact that the means are closer to the modal thicknesses in autumn. The percentage of surface ridging is fairly uniform, no doubt because deformation occurs in the early stages of ice formation in all regions and seasons. The highest percentages of ridging are observed in the western Weddell Sea, but most other regions show considerable uniformity. Ridge height on the other hand, shows some seasonal variability which mirrors the average thickness values. The snow cover thickness is quite variable regionally and seasonally, generally showing a gradual seasonal increase from autumn through to summer maximum.

[26] The tails on the distribution curves show very little seasonal variability, except in summer when there is clearly a higher percentage of thick ice present. This indicates that a
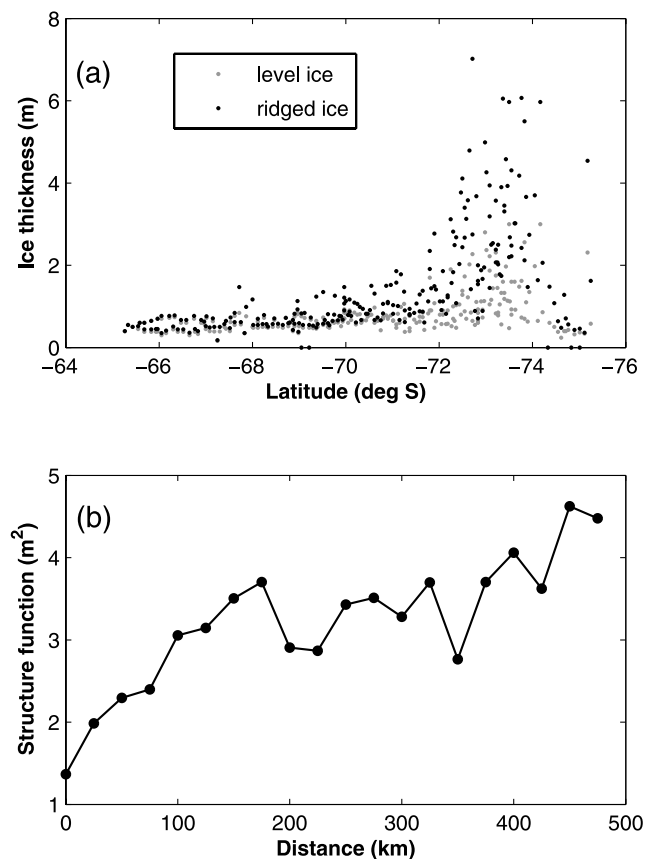
Figure 5. (a) The ice thickness along a north-south transect through the pack ice at 165°W. The grey data points show the level ice thickness and the black data points show the total average thickness including ridges calculated as described in section 2.2. (b) The structure function for total sea ice thickness along a north-south transect through the pack ice at 165°W.

fairly constant percentage of the thicker ice tends to survive the summer melt in all regions. Although the ice thickness distributions are only plotted to 4.2 m, much thicker ice is recorded in the ASPeCt observations. The greatest thicknesses calculated from the ship observations using the ridging model described in section 2.2 is 27 m in the western Weddell Sea, which is consistent with the extremely thick ice observed from upward-looking sonar aboard the Autosub in the same region (Brandon, personal communication). The snow cover thickness is also greatest in summer in all regions.

3.1.2. Regional Variability

[27] The ice thickness distribution shows least variability in the western Weddell Sea. This region contains up to 80% of the multiyear ice that survives the summer season and is therefore ice covered most of the year. The high open water fraction in summer is anomalous and results largely from one voyage that reached the Ronne polynya in a particularly low ice year (see Table 1). These values therefore reflect the higher percentage of open water in the region [*Ackley*, 1979] compared to the autumn and winter values when higher concentration and thicker ice are found in the more northern parts of the region. We note also that this south to north

thickening of the ice, due to the drift pattern in the western Weddell Sea is also exceptional, as most Antarctic areas have thinner ice in the north and thicker ice in the south [e.g., *Worby et al.*, 1998].

[28] The eastern Weddell Sea represents the most expansive sector of the Antarctic sea ice zone, extending more than 2000 km from the coast at maximum extent [*Gloersen et al.*, 1992], yet it has characteristics closer to those of the East Antarctic sectors than the western Weddell Sea. The eastern Weddell, Indian and Pacific sectors all have similar annual cycles of thickness variability as well as similar mean annual thicknesses. On the basis of the ice drift patterns reported by *Heil and Allison* [1999], it is likely that thicker ice is sometimes advected into the eastern Weddell from the west, and into the Pacific sector from the east, but our observations do not explicitly capture any seasonal impact this may have on regional distributions. It may however explain the lower annual average thickness value in the Indian Ocean sector. The Ross Sea generally has thicker ice in all seasons, except spring, when a large polynya opens adjacent to the Ross Ice Shelf. The ice thickness distribution in the Ross Sea is also affected by the advection of thicker ice from the Amundsen and Bellingshausen Seas, which have seasonal distributions close to that of the western Weddell Sea. The Amundsen and Bellingshausen Seas also have a high percentage of thick ice that survives the summer melt season and supports some of the thickest snow cover observed around the continent.

3.2. Scales of Sea Ice Thickness Variability

[29] Mapping and future assimilation of sea ice thickness fields requires additional knowledge about the spatial scales of variability for sea ice thickness and an estimate of the local noise variance (ε_o). These parameters can be estimated from the structure function of sea ice thickness, G [*Barnett et al.*, 1977; *Olea*, 1977; *Curran*, 1988], which is given by

$$G(\delta) = \frac{1}{2} < [z(x) - z(x + \delta)]^2 >, \qquad (7)$$

where z is the ice thickness at along-track locations x, and δ is an along-track lag-distance between samples. Arrow brackets denote the average over the sample space. For small δ, G provides an estimate of the local variability $\varepsilon_o = 0.5*G(0)$, which is usually small. In contrast, for large δ, G typically asymptotes to a value equal to $2.0*(\nu + \varepsilon_o)$, where ν represents the variance (note that *Curran* [1988] discusses examples where this is not the case). The lag-distance, h, at which this function reaches its asymptotic value, is the decorrelation length scale, which serves as a convenient description of the dominant length scale for the field. The strong north/south structure of sea ice thickness at certain locations [*Jeffries and Aldophs*, 1997] combined with the generally zonal nature of the circumpolar sea ice field [e.g., *Comiso*, 2003] suggests that sea ice field is likely highly anisotropic, with different spatial scales of variability expected in the north/south and east/west directions. Because there is only a limited number of north/south and east/west oriented sections available in the ASPeCt archive for analysis, we only provide annual/hemispheric estimates of the north/south and east/west length scales, $h_{n/s}$ and $h_{e/w}$.
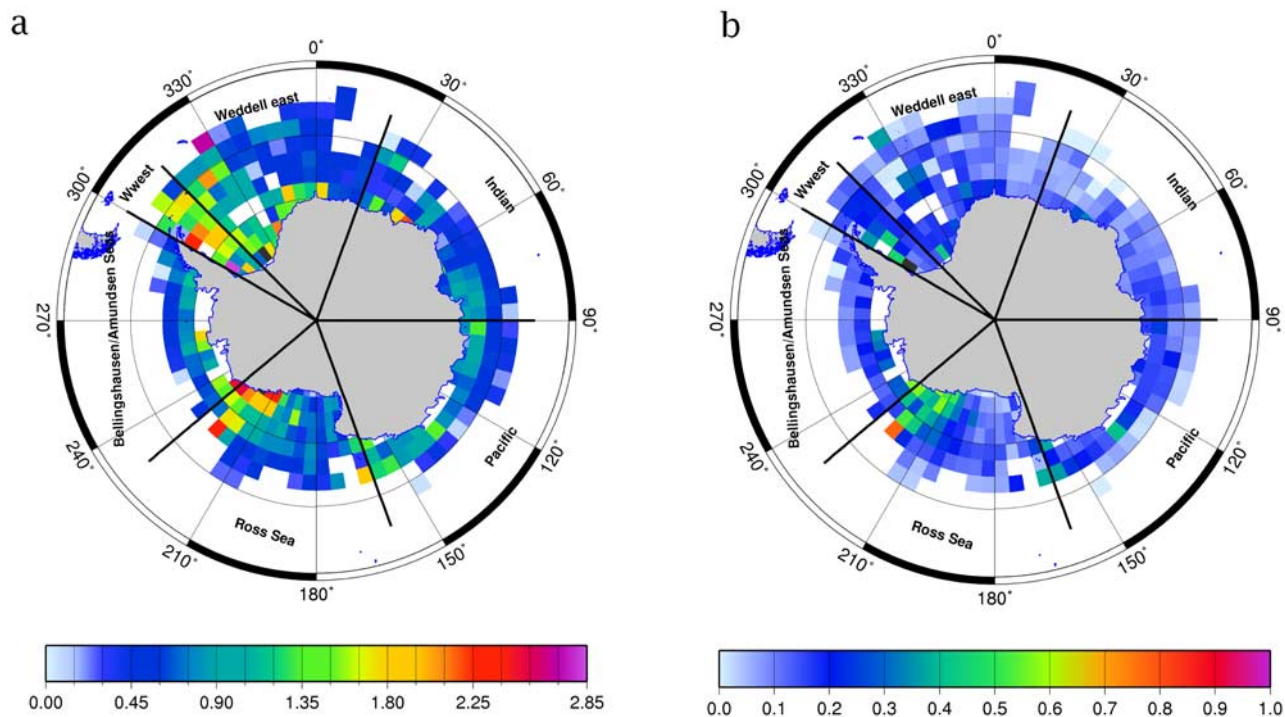
Figure 6. Circumpolar maps of (a) mean annual sea ice thickness (including ridges) and (b) mean annual snow thickness on a 2.5° latitude ×5.0° longitude grid. The data are not weighted to include the open water area.

[30] An example of a north/south ice thickness section along 165°W in the Ross Sea during December–January 1998 is presented in Figure 5a, with the grey data points representing the level ice thickness, and the black data points showing the total thickness including ridges calculated from the ship observations as described in section 2.2. The structure function of total ice thickness for this transect is shown in Figure 5b. The best estimate of ε_o, based on these data is 0.71 m^2 and the structure function asymptotes to a mean squared difference (MSD) of approximately 3.7 m^2 at a lag of ~180 km. The structure function gives a variance value consistent with the basin wide estimate of 0.84 m^2 for the Ross Sea in summer as shown in Table 3. Estimates of the local variability and the variance for each season and sector are shown in Table 3.

[31] Examination of many individual structure functions typically revealed $h_{n/s}$ values of ~100–300 km. In contrast, structure functions for the predominantly zonally oriented sea ice field surrounding Antarctica tended to lack a dominant east/west ($h_{e/w}$) scale. These "aspatial" structure functions [Curran, 1988] tend to asymptote quickly to a specific value and are relatively flat, indicating that the user has considerable latitude when choosing to average the data in the east/west direction. However, in places where east/west structure did occur, values very similar to $h_{n/s}$ were noted, suggesting that when creating ice thickness maps, a resolution of ~250 km (or 5° longitude) is probably optimal.

[32] We do not present the same analysis of the length scales of snow cover thickness on sea ice, primarily because

the ASPeCt snow thickness observations are conducted only over the level portion of the ice floes. Thus they do not reflect the extreme values that would be expected over ridged ice, where snow thickness between ridges is much higher, and zero on top of ridge sails. This is discussed in greater detail by *Worby et al.* [2008] and below.

3.3. Sea Ice and Snow Cover Thickness Maps

[33] It is increasingly common in the oceanographic community to use least-squares optimal interpolation or objective analysis [*Gandin*, 1965; *Bretherton et al.*, 1976; *Emery and Thomson*, 1997] to produce regional maps of properties such as temperature, salinity, and dynamic height. Implicit in these analyses is the requirement for knowledge of ν, ε_o, and h as described in the previous section. These techniques are also generally applicable to sea ice mapping, however, given the regional differences observed in ν, ε_o, and h for the ice thickness, and given the limited observational basis for the analysis, these techniques were not deemed practical at this early stage in our knowledge of the ice thickness field. However, guided by our best overall estimate of the decorrelation length scale (h~250 km radius for the north/south and east/west directions) we have produced 2.5° latitude × 5.0° longitude bin-averaged grids of annual mean sea ice thickness as shown in Figure 6a. The mean annual snow cover thickness is presented in Figure 6b but for reasons described above must be taken as a lower limit.

[34] The circumpolar maps are generally continuous, with some small gaps. Figure 6a clearly shows the western Weddell Sea and eastern Ross Sea as the areas of greatest

ice thickness, consistent with the distributions presented in Figure 4. Mean sea ice thicknesses in the western Weddell Sea range from less than 1 m in the south to a range of 1.5–2.5 m in most cells along the Antarctic Peninsula. Similar thicknesses are observed in the eastern Ross Sea, close to the coast. Like most areas of the sea ice zone around Antarctica the sea ice in the eastern Ross Sea gradually thickens from north to south, whereas the southern part of the western Weddell thickens from south to north in response to the dynamic effects of the Weddell gyre. Most of the sea ice around the Indian and Pacific sectors ranges from 0.3 to 0.5 m near the ice edge to values closer to a meter near the coast. There are exceptions to this in some areas where coastal effects such as iceberg tongues or polynyas may increase or decrease sea ice thickness locally. A small number of cells appear to show anomalously thick values, particularly near the ice edge, which can be attributed to observations of thicker ice being advected out of the Weddell and Ross Seas. The snow cover thickness is remarkably uniform nearly everywhere, except for slight increases in the western Weddell and eastern Ross Seas. This most likely reflects the fact that the observations are made over the level portion of ice floes, but perhaps also indicates the ubiquitous nature of snow ice formation around the continent which effectively defines a maximum thickness to which the snow cover can accumulate.

4. Discussion and Conclusions

[35] While the ASPeCt data set has significant regional and seasonal gaps, it represents the most comprehensive data set available on Antarctic sea ice thickness and offers valuable insights into the seasonal evolution of the thickness distribution around the continent. Since it is not possible to estimate the long-term (interannual or decadal) variability for the sea ice thickness field from the ASPeCt data set, we have focused on providing seasonal, and where possible, regional estimates of statistics. It must therefore be emphasized that the summary statistics presented in Table 3 comprise data collected over more than 2 decades of activity and from relatively large geographic regions and therefore represent more of a mean thickness climatology, rather than the conditions at any specific location or time within a region. In order to capture the true thickness distribution, the ship observations of surface ridging are incorporated into a simple ridge model used to calculate the total ice thickness. The resulting ice thickness distributions provide a broad overview of regional and seasonal variability in sea ice thickness around the continent, as well as the snow cover over the undeformed component of the pack.

[36] The long-term mean and standard deviation of total Antarctic sea ice thickness is 0.87 ± 0.91 m. This value is 40% higher than the mean level ice thickness (0.62 m) which we interpret as the significant influence of deformation processes on the thickness distribution of Antarctic sea ice. We also note here that the standard deviation of the total thickness is greater than the mean, indicating the highly variable nature of the ice thickness field in Antarctica, both seasonally and regionally. We conclude that characterizing the thickness of Antarctic sea ice with a single mean value therefore misrepresents the significant variability in thickness and therefore in growth, decay and

metamorphic processes that are necessary to accurately represent the evolution of the ice cover on an annual basis. These variable processes are however, reflected well in the regional ice thickness distributions that are now available from the analysis of the ASPeCt data archive.

[37] Some of the apparent discrepancies in the regional and seasonal statistics may be caused by sampling biases. In particular, there are some regions of particularly thick ice that cannot be penetrated by ships, however the introduction of aircraft observations has helped in these regions. *Timmermann et al.* [2004] showed that on a basin-wide scale (using the same sectors defined here) there is good agreement between the ASPeCt observations and the ORCA2-LIM coupled sea ice-ocean model, except in the western Weddell Sea, once differences caused by anomalous NCEP forcing in the Antarctic Peninsula region were removed.

[38] Overall, the ASPeCt sea ice data set provides highly valuable information on the sea ice and snow thickness distributions around Antarctica and represents the most comprehensive data archive on Antarctic sea ice characteristics. While further effort is required to improve the coverage of observations, the description of the spatial and temporal variability of the sea ice thickness field presented here significantly improves our understanding of the dynamics of sea ice development and evolution. In addition, robust statistics will help to optimize future sampling strategies for measuring sea ice thickness and are also a necessary prerequisite for future efforts at assimilating sea ice thickness data into sea ice models. With the release of this climatology we are hoping to explore, through intercomparisons with other measurement and modeling efforts, ways of improving our understanding of the sea ice thickness distribution around Antarctica.

Appendix A: Development of the Ridging Model

[39] The keel to sail ratio of 4.4 described in section 2.2 is derived as follows. We first define the ratio, r, as the thickness of ice below sea level to the thickness of ice plus snow above sea level,

$$r = \frac{Z_i \rho_i + Z_s \rho_s}{(Z_i + Z_s) - (Z_i \rho_i + Z_s \rho_s)}, \quad (A1)$$

where Z_i is ice thickness, Z_s is snow thickness, ρ_i is ice density and ρ_s is snow density. For snow-free level ice in hydrostatic equilibrium $r \sim 9$, but this quickly decreases when a snow cover is added, or when the ice is ridged since up to 30% of the ridge can be ice-free void space [e.g., *Leppäranta et al.*, 1995]. To determine r in the vicinity of ridges, data from nine drilled thickness transects published by *Worby and Massom* [1995] were examined. The selected transects were over a variety of ice thickness classes, each with a ridge height in the range 0.5–2.0 m. The combined total of 339 drill holes had a mean ice and snow thickness of 1.18 and 0.16 m, respectively. Using a sea ice density of 900 kg m^{-3} and a snow density of 360 kg m^{-3} (see details below), equation (A1) is used to calculate a value of $r = 5.1$ in areas of ridged ice.

[40] The effect of snowdrifts around ridges was also removed, since the presence of a snow cover causes errors in both the observations and model. In particular, observers

may not be able to differentiate ridge sails from adjoining snow drifts, hence the observations of the percent coverage (and to a lesser extent, height) of ridging will include the fraction covered by snow. To correct for this we remove the snow from the calculation using the mean ice and snow thicknesses from the ridged profiles, such that

$$r' = \left(1 - \frac{0.16}{1.18}\right)r = 4.4. \qquad (A2)$$

[41] The value $r' = 4.4$ is the final keel to sail ratio, and compares well with the value of 4.0 used by *Dierking* [1995] based on drilled measurements reported by *Lange and Eicken* [1991] and *Wadhams et al.* [1987] in the Weddell Sea. *Tin et al.* [2003] suggest an alternative model for calculating the mass of ice in ridges, but incorrectly assert that the model presented here (first presented in a technical report by *Worby and Allison* [1999]) ignores the hydrostatic effect of the ice surrounding ridges and therefore significantly underestimates the mass of ice in ridges. This is not correct since our value r' was derived empirically from drilled measurements which are, of course, representative of any hydrostatic effect the surrounding ice may have at the measurement location. *Tin et al.* [2003] also introduce the complexity of ridge sails and keels being dissociated from each other, based on observations in drilled transects that keels and sails can be mutually exclusive features. While acknowledging that drilled transects do occasionally show such features, they are nearly always small, and in most cases an artifact of the linear, two-dimensional nature of the drilled transects. Despite these differences, the revised model of *Tin et al.* [2003] produces a result almost identical to this work.

[42] The sea ice density used in the model is 900 kg m^{-3} based on work by *Buynitskiy* [1967] who published mean densities from East Antarctic sea ice for summer and winter ice of 875 kg m^{-3} and 920 kg m^{-3} respectively. *Buynitskiy* [1967] attributed the seasonal change to more porous ice in the summer months due to melt, however it may also be due to brine drainage when sampling warmer ice. Theoretical arguments suggest that warmer ice will have a higher density for constant salinity and air bubble content [*Schwerdtfeger*, 1963], but the dependence of ice density on temperature diminishes rapidly with decreasing temperature. The snow density (ρ_s) value for the model of 360 kg m^{-3} was derived from data collected on voyages to the Antarctic in 1992 and 1995 and reported by *Massom et al.* [2001]. Values ranged from 120 to 760 kg m^{-3} for different snow types with an average of 360 ± 120 kg m^{-3}.

References

Ackley, S. F. (1979), Mass-balance aspects of Weddell Sea pack ice, *J. Glaciol.*, 24(90), 391–405.

Allison, I., and A. P. Worby (1994), Seasonal changes of sea-ice characteristics off East Antarctica, *Ann. Glaciol.*, 20, 195–201.

Allison, I., R. E. Brandt, and S. G. Warren (1993), East Antarctic sea ice: Albedo, thickness distribution and snow cover, *J. Geophys. Res.*, 98(C7), 12,417–12,429.

Barnett, T. P., R. A. Knox, and R. A. Weller (1977), Space/time structure of the near-surface temperature field during the NORPAX Pole Experiment, *J. Phys. Oceanogr.*, 7, 572–579.

Brandt, R. E., S. G. Warren, A. P. Worby, and T. C. Grenfell (2005), Surface albedo of the Antarctic sea ice zone, *J. Clim.*, 18(17), 3606–3622.

Bretherton, F. P., R. E. Davis, and C. B. Fandry (1976), A technique for objective analysis and design of oceanographic experiments applied to MODE-73, *Deep Sea Res.*, 23, 559–582.

Buynitskiy, V. K. (1967), Structure, principal properties and strength of Antarctic sea ice, *Sov. Antarct. Exped. Inf. Bull., Engl. Transl.*, 65, 504–510.

Casarini, M. P. (1992), *Winter Weddell Gyre Study Polarstern (ANT VIII/2) 1989: Ice Observations Log*, 171 pp., Scott Polar Res. Inst., Cambridge, U.K.

Comiso, J. C. (2003), Large-scale characteristics and variability of the global sea ice cover, in *Sea Ice: An Introduction to its Physics, Biology, Chemistry, and Geology*, edited by D. Thomas and G. S. Dieckmann, pp. 112–142, Blackwell Sci., Oxford, U.K.

Curran, P. J. (1988), The semivariogram in remote sensing: An introduction, *Remote Sens. Environ.*, 24, 493–507.

Dierking, W. (1995), Laser profiling of the ice surface topography during the Winter Weddell Gyre Study 1992, *J. Geophys. Res.*, 100(C3), 4807–4820.

Emery, W. J., and R. E. Thomson (1997), *Data Analysis Methods in Physical Oceanography*, 634 pp., Pergamon, Oxford, U.K.

Fichefet, T., and M. A. Morales Marqueda (1999), Modelling the influence of snow accumulation and snow-ice formation on the seasonal cycle of the Antarctic sea ice cover, *J. Clim. Dyn.*, 15, 251–268.

Flato, G. M. (2004), Sea-ice modelling, in *Mass Balance of the Cryosphere*, edited by J. L. Bamber, and A. J. Payne, pp. 367–392, Cambridge Univ. Press, Cambridge, U.K.

Gandin, L. S. (1965), *Objective Analysis of Meteorological Fields*, translated from Russian, 238 pp., Isr. Program for Sci. Transl., Jerusalem.

Geiger, C. A. (2006), Propagation of uncertainties in sea ice thickness calculations from basin-scale operational observations, *TR-06-16*, 32 pp., Cold Reg. Res. and Eng. Lab., U. S. Army Corps of Eng., Hanover, N. H.

Gloersen, P., W. J. Campbell, D. J. Cavalieri, J. C. Comiso, C. L. Parkinson, and H. J. Zwally (1992), Arctic and Antarctic sea ice, 1978–1987: Satellite passive-microwave observations and analysis, *NASA Spec. Publ.*, 511, 290 pp.

Haas, C. (1998), Evaluation of ship-based electromagnetic-inductive thickness measurements of summer sea-ice in the Bellingshausen and Amundsen Seas, Antarctica, *Cold Reg. Sci. Technol.*, 27, 1–16.

Haas, C. (2003), Dynamics versus thermodynamics: The sea ice thickness distribution, in *Sea Ice: An Introduction to its Physics, Chemistry, Biology and Geology*, edited by D. N. Thomas, and G. S. Dieckman, pp. 82–111, Blackwell, Oxford, U.K.

Heil, P., and I. Allison (1999), The pattern and variability of Antarctic sea-ice drift in the Indian Ocean and western Pacific sectors, *J. Geophys. Res.*, 104(C7), 15,789–15,802.

Heil, P., I. Allison, and V. I. Lytle (1996), Seasonal and interannual variations of the oceanic heat flux under a landfast Antarctic sea ice cover, *J. Geophys. Res.*, 101(C11), 25,741–25,752.

Hibler, W. D., III. (1979), A dynamic thermodynamic sea ice model, *Mon Weather Rev.*, 9(4), 815–846.

Hibler, W. D., III (1980), Modelling a variable thickness sea ice cover, *Mon. Weather Rev.*, 108(12), 1943–1973.

Hibler, W. D., III, and S. F. Ackley (1983), Numerical simulation of the Weddell Sea pack ice, *J. Geophys. Res.*, 88(C5), 2873–2887.

Hibler, W. D., III, S. J. Mock, and W. B. Tucker III (1974), Classification and variation of sea ice ridging in the western Arctic Basin, *J. Geophys. Res.*, 79(18), 2735–2743.

Jeffries, M. O., and U. Aldophs (1997), Early winter snow and ice thickness distribution, ice structure, and development of the western Ross Sea pack ice between the ice edge and the Ross Ice Shelf, *Antarct. Sci.*, 9(2), 188–200.

Jeffries, M. O., and W. F. Weeks (1992), Structural characteristics and development of sea ice in the western Ross Sea, *Antarct. Sci.*, 5(1), 63–75.

Jeffries, M. O., A. P. Worby, K. Morris, and W. F. Weeks (1997), Seasonal variations in the properties and structural composition of sea ice and snow cover in the Bellingshausen and Amundsen Seas, Antarctica, *J. Glaciol.*, 43(143), 138–151.

Johannsen, O. M., M. Miles, and E. Bjørgo (1995), The Arctic's shrinking sea ice cover, *Nature*, 376, 126–127.

Knuth, M. A., and S. F. Ackley (2006), Summer and early fall sea ice concentration in the Ross Sea: Comparison of in situ ASPeCt observations and satellite passive microwave estimates, *Ann. Glaciol.*, 44, 303–306.

Lange, M. A., and H. Eicken (1991), The sea-ice thickness distribution in the northwestern Weddell Sea, *J. Geophys. Res.*, 96(C3), 4821–4837.

Lange, M. A., P. Schlosser, S. F. Ackley, P. Wadhams, and G. S. Dieckmann (1990), ^{18}O concentrations in sea ice of the Weddell Sea, Antarctica, *J. Glaciol.*, 36(124), 315–323.

Leppäranta, M., M. Lensu, P. Kosloff, and B. Veitch (1995), The life story of a first-year sea ice ridge, *Cold Reg. Sci. Technol.*, 23, 279–290.

Lytle, V. I., and S. F. Ackley (1996), Heat flux through sea ice in the western Weddell Sea: Convective and conductive transfer processes, *J. Geophys. Res.*, 101(C4), 8853–8868.

Mackintosh, N. A. (1972), Sea Ice Limits, *Discovery Rep.*, 36, 1–94.

Mackintosh, N. A., and H. F. P. Herdman (1940), Distribution of the pack-ice in the Southern Ocean, *Discovery Rep.*, 19, 285–296.

Maksym, T., and M. O. Jeffries (2000), A one-dimensional percolation model of flooding and snow-ice formation on Antarctic sea ice, *J. Geophys. Res.*, 105(C11), 26,313–26,331.

Massom, R. A., et al. (2001), Snow on Antarctic sea ice, *Rev. Geophys.*, 39(3), 413–445.

Maykut, G. A. (1978), Energy exchange over young sea ice in the central Arctic, *J. Geophys. Res.*, 83(C7), 3646–3658.

Olea, R. A. (1977), Measuring spatial dependence with semi-variograms, report, 29 pp., Kans. Geol. Survey, Campus West, Lawrence.

Parkinson, C. L. (1990), Search for the little ice age in Southern Ocean sea ice records, *Ann. Glaciol.*, 14, 221–225.

Parkinson, C. L., D. J. Cavalieri, P. Gloersen, H. J. Zwally, and J. C. Comiso (1999), Arctic sea ice extents, areas, and trends, 1978–1996, *J. Geophys. Res.*, 104(C9), 20,837–20,856.

Reid, J. E., J. Vrbancich, and A. P. Worby (2003), A comparison of ship-borne and airborne electromagnetic methods for Antarctic sea ice thickness measurements, *Explor. Geophys.*, 34, 46–50.

Roberts, A., I. Allison, and V. I. Lytle (2001), Sensible- and latent-heat-flux estimates over the Mertz Glacier polynya, East Antarctica, from in-flight measurements, *Ann. Glaciol.*, 33, 377–384.

Rothrock, D. A., Y. Yu, and G. A. Maykut (1999), Thinning of the Arctic sea-ice cover, *Geophys. Res. Lett.*, 26(23), 3469–3472.

Rothrock, D. A., J. Zhang, and Y. Yu (2003), The Arctic ice thickness anomaly of the 1990s: A consistent view from observations and models, *J. Geophys. Res.*, 108(C3), 3083, doi:10.1029/2001JC001208.

Schwerdtfeger, P. (1963), The thermal properties of sea ice, *J. Glaciol.*, 4(36), 789–807.

Serreze, M. C., J. A. Maslanik, T. A. Scambos, F. Fetterer, J. Stroeve, K. Knowles, C. Fowler, S. Drobot, R. G. Barry, and T. M. Harran (2003), A record minimum arctic sea ice extent and area in 2002, *Geophys. Res. Lett.*, 30(3), 1110, doi:10.1029/2002GL016406.

Serreze, M. C., M. M. Holland, and J. Stroeve (2007), Perspectives on the Arctic's shrinking sea ice cover, *Science*, 315(5818), 1533–1536.

Strass, V. H., and E. Fahrbach (1998), Temporal and regional variation of sea ice draft and coverage in the Weddell Sea obtained from upward looking sonars, in *Antarctic Sea Ice: Physical Processes, Interactions and Variability*, *Antarct. Res. Ser.*, vol. 74, edited by M. O. Jeffries, pp. 123–139, AGU, Washington, D. C.

Thorndike, A. S., D. A. Rothrock, G. A. Maykut, and R. Colony (1975), The thickness distribution of sea ice, *J. Geophys. Res.*, 80(33), 4501–4513.

Timmermann, R., A. P. Worby, H. Goosse, and T. Fichefet (2004), Utilizing the ASPeCt sea ice thickness data set to evaluate a global coupled sea ice-ocean model, *J. Geophys. Res.*, 109, C07017, doi:10.1029/2003JC002242.

Tin, T., M. O. Jeffries, M. Lensu, and J. Tuhkuri (2003), Estimating the thickness of ridged sea ice from ship observations in the Ross Sea, *Antarct. Sci.*, 15(1), 47–54.

Tucker, W. B., III, and J. W. Govoni (1981), Morphological investigations of first-year sea ice pressure ridge sails, *Cold Reg. Sci. Technol.*, 5, 1–12.

Tucker, W. B., J. W. Weatherly, D. T. Eppler, L. D. Farmer, and D. L. Bentley (2001), Evidence for rapid thinning of sea ice in the western Arctic Ocean at the end of the 1980s, *Geophys. Res. Lett.*, 28(14), 2851–2854.

Wadhams, P., and N. R. Davis (2000), Further evidence of ice thinning in the Arctic Ocean, *Geophys. Res. Lett.*, 27(24), 3973–3975.

Wadhams, P., M. A. Lange, and S. F. Ackley (1987), The ice thickness distribution across the Atlantic sector of the Antarctic Ocean in midwinter, *J. Geophys. Res.*, 92(C13), 14,535–15,552.

Weeks, W. F., and S. F. Ackley (1986), The growth, structure and properties of sea ice, in *The Geophysics of Sea Ice*, *NATO ASI Ser. B, Phys.*, vol. 146, edited by N. Untersteiner, pp. 9–164, Plenum, New York.

Worby, A. P. (1999), *Observing Antarctic Sea Ice: A Practical Guide for Conducting Sea Ice Observations From Vessels Operating in the Antarctic Pack Ice* [CD-ROM], Aust. Antarct. Div., Hobart, Tasmania, Australia.

Worby, A. P., and I. Allison (1991), Ocean-atmosphere energy exchange over thin variable concentration Antarctic pack ice, *Ann. Glaciol.*, 15, 184–190.

Worby, A. P., and I. Allison (1999), A technique for making ship-based observations of Antarctic sea ice thickness and characteristics: Part I. Observational technique and results, *Res. Rep. 14*, pp. 1–23, Antarct. Coop. Res. Cent., Univ. of Tasmania, Hobart, Tasmania, Australia.

Worby, A. P., and V. Dirita (1999), A technique for making ship-based observations of Antarctic sea ice thickness and characteristics: Part II. User operating manual, *Res. Rep. 14*, pp. 23–63, Antarct. Coop. Res. Cent., Univ. of Tasmania, Hobart, Tasmania, Australia.

Worby, A. P., and R. A. Massom (1995), The structure and properties of sea ice and snow cover in East Antarctic pack ice, *Res. Rep. 7*, 177 pp., Antarct. Coop. Res. Cent., Univ. of Tasmania, Hobart, Tasmania, Australia.

Worby, A. P., M. O. Jeffries, W. F. Weeks, K. Morris, and R. Jaña (1996), The thickness distribution of sea ice and snow cover during late winter in the Bellingshausen and Amundsen Seas, Antarctica, *J. Geophys. Res.*, 101(C12), 28,441–28,455.

Worby, A. P., R. A. Massom, I. Allison, V. I. Lytle, and P. Heil (1998), East Antarctic sea ice: A review of its structure, properties and drift, in *Antarctic Sea Ice: Physical Processes, Interactions and Variability*, *Antarct. Res. Ser.*, vol. 74, edited by M. O. Jeffries, pp. 41–67, AGU, Washington, D. C.

Worby, A. P., G. M. Bush, and I. Allison (2001), Seasonal development of the sea-ice thickness distribution in East Antarctica: Measurements from upward-looking sonar, *Ann. Glaciol.*, 33, 177–180.

Worby, A., T. Markus, A. Steer, V. Lytle, and R. Massom (2008), Evaluation of AMSR-E snow depth product over East Antarctic sea ice using in situ measurements and aerial photography, *J. Geophys. Res.*, doi:10.1029/2007JC004181, in press.

World Meteorological Organization (1970), *Sea ice nomenclature: Terminology, Codes and Illustrated Glossary*, WMO/OMM/BMO 259, TP 145, World Meteorological Organization, Geneva.

Yu, Y., G. A. Maykut, and D. Rothrock (2004), Changes in the thickness distribution of Arctic sea ice between 1958–1970 and 1993–1997, *J. Geophys. Res.*, 109, C08004, doi:10.1029/2003JC001982.

————————————
S. F. Ackley, Department of Earth Science and Environmental Sciences, University of Texas at San Antonio, 1 UTSA Circle, San Antonio, TX 78249, USA.

T. L. DeLiberty and C. A. Geiger, Department of Geography, University of Delaware, Newark, DE 19716, USA.

M. J. Paget, Commonwealth Scientific and Industrial Research Organization, Canberra, ACT 2601, Australia.

M. L. Van Woert, National Science Foundation, Office of Polar Programs, 4201 Wilson Boulevard, Arlington, VA 22230, USA.

A. P. Worby, Australian Antarctic Division and Antarctic Climate and Ecosystems Cooperative Research Center, 203 Channel Highway, Kingston, Tas 7050, Australia. (a.worby@utas.edu.au)